Correlation between degree of crystallinity and bluing of Zn1–Co Al2O4 (0≤x≤1) nanopowders prepared by soft chemistry route

Youssef El Jabbar, Hind Lakhlifi, Rachida El Ouatib, Lahcen Er-Rakho, Sophie Guillemet-Fritsch, Yann Borjon-Piron, Bernard Durand

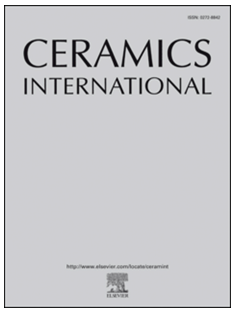

Correlation between degree of crystallinity and bluing of $Zn_{1-x}Co_xAl_2O_4$ ($0 \le x \le 1$) nanopowders prepared by soft chemistry route

Youssef El Jabbar, Hind Lakhlifi, Rachida El Ouatib, Lahcen Er-Rakho, Sophie Guillemet-Fritsch, Yann Borjon-Piron, Bernard Durand

PII: S0272-8842(21)00581-2

DOI: https://doi.org/10.1016/j.ceramint.2021.02.205

Reference: CERI 27998

To appear in: *Ceramics International*

Received Date: 2 January 2021

Revised Date: 17 February 2021

Accepted Date: 21 February 2021

Please cite this article as: Y. El Jabbar, H. Lakhlifi, R. El Ouatib, L. Er-Rakho, S. Guillemet-Fritsch, Y. Borjon-Piron, B. Durand, Correlation between degree of crystallinity and bluing of $Zn_{1-x}Co_xAl_2O_4$ ($0 \le x \le 1$) nanopowders prepared by soft chemistry route, *Ceramics International*, https://doi.org/10.1016/j.ceramint.2021.02.205.

Correlation between degree of crystallinity and bluing of $Zn_{1-x}Co_xAl_2O_4$ ($0 \leq x \leq 1$) nanopowders prepared by soft chemistry route

Youssef El Jabbar[a,*], Hind Lakhlifi[a], Rachida El Ouatib[a], Lahcen Er-Rakho[a], Sophie Guillemet-Fritsch[b], Yann Borjon-Piron[b], Bernard Durand[b]

[a] Laboratoire de Physico-chimie des Matériaux Inorganiques, Faculté des sciences Aïn chock, Université Hassan II, Bb. 5366 Mâarif, Casablanca, Morocco.

[b] Institut Carnot CIRIMAT, CNRS Université de Toulouse, 118 route de Narbonne, 31062 Toulouse Cedex 9, France.

* Corresponding author email: ysf.eljabbar@gmail.com (youssef El Jabbar)

Abstract

In this article, we report a facile precursor pyrolysis by sol-gel method to prepare spinel-type Cobalt-substituted zinc aluminate nanoparticles ($Zn_{1-x}Co_xAl_2O_4$, $0 \leq x \leq 1$). The relationship between the degree of crystallinity and the optical properties under the effect of the calcination temperature was investigated. The synthesized powders were characterized by means of X-ray diffraction (XRD), Thermogravimetry and Differential thermal analysis (TG–DTA), field emission scanning electron microscopy (FE-SEM), Brunauer–Emmett–Teller analysis (BET), UV–Vis absorption spectroscopy analysis and colorimetric analysis (CIELab). A single-phase $Zn_{1-x}Co_xAl_2O_4$ ($0 \leq x \leq 1$) spinel was formed at an annealing temperature of 700°C. Structural refinement via the Rietveld method shows that an annealing temperature in excess of 700°C leads to a decrease in the amorphous phase rate. At 800 °C, the enrichment in 50% of cobalt leads to blue powders with a degree of crystallinity of approximately 92% and a quasi-spherical morphology of nanometric size less than 100 nm.

Keywords: Zinc-cobalt aluminate; Amorphous phase; Ceramics; Nanocrystals; Colorimetric analysis.

1. Introduction

Inorganic pigments have wide industrial applications. In fact, they are used to colour and decorate plastics, rubber, glasses, cement, glazes, ceramics, porcelain enamels, etc. Among these materials, the transition metal oxides which generally have different colours. Their absorption properties are governed by the degree of oxidation of the transition metal and by its environment in the crystal lattice [1–4]. Usually the main source of the blue colour is the cobalt that can be introduced in different structures, such as Co_2SiO_4 (olivine) [5], $(Co, Zn)_2SiO_4$ (willemite) [6,7] and $CoAl_2O_4$ (cobalt spinel) [8]. Admittedly, the use of cobalt-based blue pigments in the ceramic industries leads to a more intense shade, after treatment at high temperature, but this metal is expensive which increases the manufacturing cost. This suggests reducing the amount of cobalt via other combinations of oxides or looking for other materials that would have almost similar optical properties [9–12]. Quite recently, considerable attention has been paid to prepare different compounds doped with other metal cations which allow to have a shades of blue colour by reducing the amount of cobalt [13–15]. Furthermore, the particle size and morphology of the powders have been shown to have an effect on the amount of pigment used in ceramic manufacturing. In fact, mixing the pigments with other compositions, such as transparent glazes, to colour objects requires a finer powder to ensure better reactivity and then better colour coverage. This can lead to reducing the amount of pigment used [16–18]. In order to meet this requirement, it is essential to choose an appropriate synthesis method. Previous works have shown that the conventional method of synthesis by solid reaction of these oxides requires heat treatment at a high temperature, for a long period of time, as well as prolonged grinding. This generally leads to powders of poor homogeneity [19–21]. In the last few years there has been a growing interest in the optimization of synthesis parameters developed by soft chemistry such as combustion route [22], hydrothermal synthesis [23], co-precipitation [24] and sol-gel [25]. These methods have

been shown to produce materials of greater homogeneity and purity at temperatures lower than those required for conventional methods.

The present paper deals with blue pigments based on the cobalt-doped $ZnAl_2O_4$ spinel. This type of oxide has the general formula AB_2O_4 in which the tetrahedral sites are occupied by the A^{2+} cations and the octahedral sites are occupied by the B^{3+} cations. It exhibits high thermal stability and high mechanical resistance [26,27]. In this study, $Zn_{1-x}Co_xAl_2O_4$ ($0 \leq x \leq 1$) solid solutions were developed using the sol-gel route with citric acid as the complexing and gelling agent. The obtained polymeric precursors were converted to metal oxides by appropriate thermal treatment. The calcination temperature was optimised to produce homogeneous single-phase powders with small particle sizes. The synthesis conditions, as well as the structural, optical and morphological characterisation, were discussed.

2. Experimental procedure

The preparation of $Zn_{1-x}Co_xAl_2O_4$ ($0 \leq x \leq 1$) nano-ceramic pigments consists in dissolving with stoichiometric proportions the following metallic nitrates: $Co(NO_3)_2 \cdot 6H_2O$ (99.0%, Sigma Aldrich), $Zn(NO_3)_2 \cdot 6H_2O$ (99.0%, Sigma Aldrich) and $Al(NO_3)_3 \cdot 9H_2O$ (99.0%, Sigma Aldrich). Citric acid (CA) was added to the mixture as a complexing agent with a molar ratio (CA/Cations) equal to 3. The pH was adjusted to 7 with an ammonia solution. The viscous gel obtained after evaporation of the mixture solution was dried at 120°C/24h then pre-calcined in air at 300°C/12h for removal organic matter (pyrolysis). The precursor obtained was ground and calcined in air at different temperatures. The calcination temperature was determined by thermogravimetry and differential thermal analysis (TGA-DTA). The heating rate was fixed at 10°C/min.

The thermal decomposition behaviors of the precursors obtained after pyrolysis were monitored by DTA-TGA analyzer (DTA-TG-60H Shimadzu). Structural phase analysis of the

synthesised powders were performed by X-ray diffraction using a diffractometer equipped with a detector Lynx Eye (Bruker D8 Advance, $\lambda_{CuK\alpha}$=1.5406 Å). The optical properties were investigated by UV–Vis spectrophotometry analysis (Perkin Elmer Lambda 35) and by colourimetric measurement using the CIE Lab system colorimeter (CR-400/410, KONICA MINOLTA). The morphology was examined by field emission scanning electron microscopy (JEOL JSM 6700F) and the specific surface area measurements were determined by the BET method (Micrometrics Flowsorb II 2300).

3. Results and Discussion

3.1. Thermal analysis

The thermal behaviour of the $Zn_{1-x}Co_xAl_2O_4$ precursors obtained at 300°C for 12 hours was followed by DTA-TGA analysis in air with a heating rate of 10°C/min. As shown in Fig.1 (a, b and c), the thermograms (TGA) for each of the compounds with x=0, x=0.5 and x=1 reveal a total weight loss about 80%. The elimination of water was manifested by a weight loss occurring between room temperature and 200°C accompanied by an endothermic effect on the DTA curves. The removal of residual organic matter in the samples was manifested by rapid weight loss on the TGA curves in the temperature range of 400-600 °C. This weight loss accompanied by strong effect on the DTA curves is due to the removal of the carbon and nitrogen oxides and it can also indicates the formation of spinel oxide. A small weight loss accompanied by a weak exothermic effect was observed around 720°C. This is probably due to the elimination of the residual organic from incomplete combustion as carbon dioxide.

3.2. X- Ray diffraction

The XRD patterns of the $Zn_{1-x}Co_xAl_2O_4$ ($0 \leq x \leq 1$) samples obtained at 500°C, 600°C and 700°C were presented in Fig.2 (a,b and c). At heating temperature of 500°C, the XRD

diagrams obtained show an amorphous phase for the compounds with $x \leq 0.5$ while crystalline phases were appeared for $x \geq 0.6$ (Fig.2 (a)). The Fig. 2 (b) shows that the heat treatment at 600 ° C leads to crystalline phases, except for the composition with $x=0$, which is still amorphous. At 700 ° C (Fig.2 (c)), all the obtained compounds have crystallized phases which can be indicate that solid solutions of the spinel structure $Zn_{1-x}Co_xAl_2O_4$ ($0 \leq x \leq 1$) were obtained. In order to verify this result, the powder x-ray diffraction patterns of the fractions x = 0, 0.5 and 1 obtained at 700°C were investigated by Rietveld refinement to provide more information on the compositions and the structural parameters. The crystal structure of $(Zn,Co)[Al]_2O_4$ corresponds to a normal spinel in which the Co^{2+} and Zn^{2+} cations only occupy the tetrahedral sites and the Al^{3+} cations occupy the octahedral sites. However, it is possible to have an inverse structure $(Zn^{2+},Co^{2+},Al^{3+})[Co^{3+}, Al^{3+}]O_4$ in which the cobalt and aluminum ions are distributed over the octahedral and tetradric sites [28,29]. The following data was considered in the refinement process:

- The phase symmetry was cubic with the space group Fd-3m.
- The cations (Zn^{2+}, Co^{2+}) and (Al^{3+}, Co^{3+}) were distributed, respectively, between the tetrahedral sites 8a and octahedral 16d.
- The refinements were carried out with isotropic thermal agitation factors Biso=1.
- The oxygen sites (32e (u, u, u)) were considered to be fully occupied.

The Rietveld refinement was carried out by using the FullProf package. The scale factor, lattice parameter, fractional coordinates of atoms in the structure model, background coefficients and isotropic displacement parameters were varied during the fitting procedure. The quality of the Rietveld fit is assessed with a number of statistical descriptors (reliability factors). Some of the commonly used residuals that need to be minimized are: Rp (profile residual), Rwp (weighted profile residual) and $\chi 2$ (goodness of fit). As shown in Table 1, the refined structural parameters (lattice parameter, atomic position, occupancy rate and thermal

agitation coefficient) lead to low reliability factors. In the compounds with x=0.5 and x=1, cobalt occupies the tetrahedral sites and the octahedral sites, which shows partial oxidation of Co^{2+} to Co^{3+}. It was probably enhanced by the oxidising environment during thermal decomposition of the nitrates [30]. The lattice parameters of the compounds with x=0 and x=1 were compatible, respectively, with the JCPDS files of $ZnAl_2O_4$ (JCPDS Card No. 05-0669) and $CoAl_2O_4$ (JCPDS Card No. 38-0814). Figure 3 presents the graphical illustration of the observed, calculated and difference signals for the composition x=0.5 prepared at 700°C. The representation of the coordination polyhedra is presented in Figure 4.

The average crystallite size (D) for the composition x = 0.5 obtained at different temperatures was deduced from the profiles of the X-ray diffraction lines and calculated via Scherrer's formula [31]. As Table 3 shows, it is noteworthy that the crystallite size increases from 20 nm at 700°C to 26 nm at 1000°C; this means that the crystallinity increases with the annealing temperature. This agrees with the evolution of the peaks as shown in fig.5. The quantification of the crystalline phases in the sample with x = 0.5—obtained at each of 700°C, 800°C, 900°C and 1000°C—was determined by the internal standard method. This process consists of mixing an exact quantity of well-crystallized α-Alumina powder as internal standard (50% by weight) with the sample to be analysed. The percentage of the crystalline phase found in the sample is calculated by undertaking Rietveld refinement of the XRD diagrams of the mixtures produced (sample and internal standard); this is facilitated by the use of FullProf software (Fig.6). The phase percentage values thus obtained were corrected with those of the prepared mixture; this makes it possible to deduce the degree of the crystalline and amount of amorphous phases in the sample (Table 2). The sample obtained at 700 ° C has been a degree of crystallinity of about 88%; this value increases as the annealing temperature increases, and this phenomenon can be explained by the introduction of amorphous alumina, under the effect of temperature, into the spinel structure [32].

3.3. Optical properties

The colour of the synthesised powders was investigated by colorimetric measurements and UV-Vis spectroscopy analysis. Table 3 presents the evolution of the values of the colorimetric parameters (L*, a* and b*) of $Zn_{1-x}Co_xAl_2O_4$ (x = 0, 0.5, and 1) powders obtained at different temperatures. It was observed that the enrichment in cobalt (x=0.5 and 1) and the annealing temperature have effects on the powders' colorimetric parameters. In fact, the brightness of the powders increases with annealing temperature and decreases for the Co-doped $ZnAl_2O_4$ compositions. The parameter (-b*), which is responsible for the bluing, increases with temperature; meanwhile, the parameter (-a*), which is responsible for green colouring, remains weak. This change in colour can likely be explained by a reduction of Co^{3+} to Co^{2+} and a change in the coordination of cobalt [30]. Furthermore, Table 3 shows that the composition x = 0.5 obtained at annealing temperatures greater than or equal to 800°C exhibits higher values of the parameter b *. This indicates that these powders exhibit intense shades of the blue colour. The CIE (x,y) chromaticity coordinates of the samples were obtained by using OSRAM colour calculator software. Fig.7 illustrates the CIE chromaticity diagram obtained for the powders with the composition x=0.5 prepared at different temperatures. It can be observed that the powders calcined at T ≥800°C are found in the domain characteristic of the blue colour. Fig.8 presents the UV-Vis absorbance spectra of the $Zn_{1-x}Co_xAl_2O_4$ (x = 0, 0.5, and 1) powders obtained at 800°C. In the visible region, the spectra of the cobalt-enriched powders (x=0.5 and x=1) show a triplet of bands at 550, 590 and 680 nm. These absorptions are ascribed to the $^4A_2(F) \rightarrow {}^4T_1(P)$ transition of Co^{2+} ions in tetrahedral symmetry which gives a blue hue to the samples [33].

3.4. Morphological properties

Powders with high specific surface areas and fine particle sizes allow for high colouring strength as they provide more reactivity during reaction mixing. Hence, the surface areas of the blue powders with the compositions x=0 and x=0.5 obtained at 800 °C, 900°C and 1000 °C were determined using the BET method. Table 4, shows that the annealing temperature leads to a low specific surface area and the $Zn_{0.5}Co_{0.5}Al_2O_4$ (x=0.5) powders have a large specific surface area compared to $CoAl_2O_4$ (x=1) powders. The maximum value was observed of 76 m^2/g for the composition x=0.5 obtained at 800 °C. The surface morphological analysis of this last composition was executed by FESEM technique, as shown in Fig. 9 (a). The powder comprises compact agglomerates of particles that feature quasi-spherical shapes and nanometric sizes of less than 100 nm. The quantitative elemental composition is resolved with energy dispersive spectroscopy (EDS) analysis. The EDS spectrum of $Zn_{0.5}Co_{0.5}Al_2O_4$ (x=0.5) nanoparticles manifests the presence of the constituents Zn, Co, Al and O solely; see Fig. 9(b). The stoichiometric ratios used for synthesis of this composition closely match corresponding EDS result. The observed slight variation may be due to the presence of the amorphous phase (Table 2).

4. Conclusion

Cobalt-substituted $ZnAl_2O_4$ powders were successfully synthesised by the sol-gel route. Citric acid was used as a complexing and gelling agent. We concluded that a 5-hour heat treatment of the precursors at 700°C derives $Zn_{1-x}Co_xAl_2O_4$ ($0 \leq x \leq 1$) aluminates that feature a spinel structure; this occurs regardless of Co content. The blueness of the cobalt-enriched powders increases with the degree of crystallinity. For the $Zn_{0.5}Co_{0.5}Al_2O_4$ composition, the calcination temperature at 800 °C was sufficient to produce a nanometric blue powder with a degree of crystallinity of 92% and exhibits a large specific surface area of about 76 m^2/g. In

consequence, this powder could be used with a reduced quantity in the ceramic pigmentation with good colour coverage.

References

[1] Q. Gao, X. Wu, Y. Fan, Q. Meng, Color performance and near infrared reflectance property of novel yellow pigment based on Fe_2TiO_5 nanorods decorated mica composites, Dyes Pigments. 146 (2017) 537–542. https://doi.org/10.1016/j.dyepig.2017.07.035.

[2] J. Li, M.A. Subramanian, Inorganic pigments with transition metal chromophores at trigonal bipyramidal coordination: $Y(In,Mn)O_3$ blues and beyond, J. Solid State Chem. 272 (2019) 9–20. https://doi.org/10.1016/j.jssc.2019.01.019.

[3] L. Verger, O. Dargaud, N. Menguy, D. Troadec, L. Cormier, Interaction between Cr-bearing pigments and transparent glaze: A transmission electron microscopy study, J. Non-Cryst. Solids. 459 (2017) 184–191. https://doi.org/10.1016/j.jnoncrysol.2017.01.016.

[4] N.V. Golubev, E.S. Ignat'eva, V.M. Mashinsky, E.O. Kozlova, V.N. Sigaev, A. Monguzzi, A. Paleari, R. Lorenzi, Pre-crystallization heat treatment and infrared luminescence enhancement in Ni^{2+}-doped transparent glass-ceramics, J. Non-Cryst. Solids. 515 (2019) 42–49. https://doi.org/10.1016/j.jnoncrysol.2019.04.006.

[5] S. Bayat, A. Sobhani, M. Salavati-Niasari, Co_2SiO_4 nanostructures: New simple synthesis, characterization and investigation of optical property, Mater. Res. Bull. 88 (2017) 248–257. https://doi.org/10.1016/j.materresbull.2016.12.043.

[6] N.M. Rasdi, Y.W. Fen, N.A.S. Omar, M.H.M. Zaid, Effects of cobalt doping on structural, morphological, and optical properties of Zn_2SiO_4 nanophosphors prepared by sol-gel method, Results Phys. 7 (2017) 3820–3825. https://doi.org/10.1016/j.rinp.2017.09.057.

[7] T. Dippong, F. Goga, E.-A. Levei, O. Cadar, Influence of zinc substitution with cobalt on thermal behaviour, structure and morphology of zinc ferrite embedded in silica matrix, J. Solid State Chem. 275 (2019) 159–166. https://doi.org/10.1016/j.jssc.2019.04.011.

[8] Y. Zhang, M. Ye, A. Han, C. Ding, J. Yang, K. Zhang, Preparation and characterization of encapsulated $CoAl_2O_4$ pigment and charge control agent for ceramic toner via suspension polymerization, Ceram. Int. 44 (2018) 20322–20329. https://doi.org/10.1016/j.ceramint.2018.08.020.

[9] E.A. Chavarriaga, A.A. Lopera, T.B. Wermuth, S. Arcaro, A. Gómez, O.J. Restrepo, J. Alarcón, C.P. Bergmann, Synthesis by solution combustion of inorganic blue pigments $MFe_2(P_2O_7)_2$: Influence of the cation M (Zn^{2+}, Co^{2+}, Cu^{2+}, and Mg^{2+}) on their optical properties, Solid State Sci. 103 (2020) 106180. https://doi.org/10.1016/j.solidstatesciences.2020.106180.

[10] Y.F. Gomes, J. Li, K.F. Silva, A.A.G. Santiago, M.R.D. Bomio, C.A. Paskocimas, M.A. Subramanian, F.V. Motta, Synthesis and characterization of Y(In, Mn)O_3 blue pigment using the complex polymerization method (CPM), Ceram. Int. 44 (2018) 11932–11939. https://doi.org/10.1016/j.ceramint.2018.04.152.

[11] J. Jing, Y. Zhang, J. Sun, X. Zhao, D. Gao, Y. Zhang, A comparative study on different RE-doped (RE= Pr, Nd, Sm)$SrCuSi_4O_{10}$ blue pigments with high near-infrared reflectance, Dyes Pigments. 150 (2018) 9–15. https://doi.org/10.1016/j.dyepig.2017.10.045.

[12] V. Jeseentharani, A. Dayalan, K.S. Nagaraja, Co-precipitation synthesis, humidity sensing and photoluminescence properties of nanocrystalline Co^{2+} substituted zinc(II) molybdate ($Zn_{1-x}Co_xMoO_4$; x = 0, 0.3, 0.5, 0.7, 1), Solid State Sci. 67 (2017) 46–58. https://doi.org/10.1016/j.solidstatesciences.2017.02.008.

[13] S. Kimura, Y. Suzuki, Synthesis of Co-lean and Co-rich $Li_2CoTi_3O_8$-based pigments: Potential Co reduction and blue-green dichroism, Ceram. Int. 45 (2019) 12602–12607. https://doi.org/10.1016/j.ceramint.2019.03.036.

[14] S.G. Menon, H.C. Swart, Microwave-assisted synthesis of blue-green $NiAl_2O_4$ nanoparticle pigments with high near-infrared reflectance for indoor cooling, J. Alloys Compd. 819 (2020) 152991. https://doi.org/10.1016/j.jallcom.2019.152991.

[15] N. Zhou, Y. Li, Y. Zhang, Y. Shu, S. Nian, W. Cao, Z. Wu, Synthesis and characterization of $Co_{1-x}Ca_xAl_2O_4$ composite blue nano-pigments by the polyacrylamide gel method, Dyes Pigments. 148 (2018) 25–30. http://dx.doi.org/10.1016/j.dyepig.2017.08.057.

[16] J. Gilabert, M.D. Palacios, V. Sanz, S. Mestre, Fuel effect on solution combustion synthesis of Co(Cr, $Al)_2O_4$ pigments, Bol. Soc. Esp. Cerámica Vidr. 56 (2017) 215–225. https://doi.org/10.1016/j.bsecv.2017.03.003.

[17] J. Gilabert, M.D. Palacios, V. Sanz, S. Mestre, Characteristics reproducibility of (Fe, Co)$(Cr,Al)_2O_4$ pigments obtained by solution combustion synthesis, Ceram. Int. 42 (2016) 12880–12887. https://doi.org/10.1016/j.ceramint.2016.05.054.

[18] Y. Tang, C. Wu, Y. Song, Y. Zheng, K. Zhao, Effects of colouration mechanism and stability of $CoAl_2O_4$ ceramic pigments sintered on substrates, Ceram. Int. 44 (2018) 1019–1025. https://doi.org/10.1016/j.ceramint.2017.10.038.

[19] B. Roy, A. Pandey, Q. Zhang, T.W. Heitmann, D. Vaknin, D.C. Johnston, Y. Furukawa, Experimental evidence of a collinear antiferromagnetic ordering in the frustrated $CoAl_2O4$ spinel, Phys. Rev. B. 88 (2013) 174415. https://doi.org/https://doi.org/10.1103/PhysRevB.88.174415.

[20] W. Bao, F. Ma, Y. Zhang, X. Hao, Z. Deng, X. Zou, W. Gao, Synthesis and characterization of Fe^{3+} doped $Co_{0.5}Mg_{0.5}Al_2O_4$ inorganic pigments with high near-infrared reflectance, Powder Technol. 292 (2016) 7–13. https://doi.org/10.1016/j.powtec.2016.01.013.

[21] X. He, F. Wang, H. Liu, L. Niu, X. Wang, Synthesis and color properties of the TiO2@ $CoAl_2O_4$ blue pigments with low cobalt content applied in ceramic glaze, J. Am. Ceram. Soc. 101 (2018) 2578–2588. https://doi.org/10.1111/jace.15422.

[22] M. Han, Z. Wang, Y. Xu, R. Wu, S. Jiao, Y. Chen, S. Feng, Physical properties of $MgAl_2O_4$, $CoAl_2O_4$, $NiAl_2O_4$, $CuAl_2O_4$, and $ZnAl_2O_4$ spinels synthesized by a solution combustion method, Mater. Chem. Phys. 215 (2018) 251–258. https://doi.org/10.1016/j.matchemphys.2018.05.029.

[23] Y. Chang, T. Feng, C. Wu, Y. Chen, K. Ke, Y. Liu, H. Wang, S. Dong, Controlled synthesis of blue spherical $CoAl_2O_4$ pigment powder in Pickering emulsion assisted with a hydrothermal process, Adv. Powder Technol. 29 (2018) 1222–1229. https://doi.org/10.1016/j.apt.2018.02.014.

[24] D.D. Andhare, S.R. Patade, J.S. Kounsalye, K.M. Jadhav, Effect of Zn doping on structural, magnetic and optical properties of cobalt ferrite nanoparticles synthesized via. Co-precipitation method, Phys. B Condens. Matter. 583 (2020) 412051. https://doi.org/10.1016/j.physb.2020.412051.

[25] P.K. Thejus, K.G. Nishanth, Rational approach to synthesis low-cost $BiVO_4$–ZnO complex inorganic pigment for energy efficient buildings, Sol. Energy Mater. Sol. Cells. 200 (2019) 109999. https://doi.org/10.1016/j.solmat.2019.109999.

[26] P. Heidari, S.M. Masoudpanah, Structural and magnetic properties of $MgFe_2O_4$ powders synthesized by solution combustion method: the effect of fuel type, J. Mater. Res. Technol. 9 (2020) 4469–4475. https://doi.org/10.1016/j.jmrt.2020.02.073.

[27] Z. Li, K. Wang, B. Ge, Z. Zhang, Z. Wei, Z. Shi, G. Qiao, Synergistic enhancement of sinterability and corrosion resistance of $ZnCr_2O_4$ spinel by TiO_2 addition for carbon-free aluminum electrolysis, Chem. Eng. J. 400 (2020) 125924. https://doi.org/10.1016/j.cej.2020.125924.

[28] D. Dwibedi, C. Murugesan, M. Leskes, P. Barpanda, Role of annealing temperature on cation ordering in hydrothermally prepared zinc aluminate ($ZnAl_2O_4$) spinel, Mater. Res. Bull. 98 (2018) 219–224. https://doi.org/10.1016/j.materresbull.2017.10.010.

[29] D. Visinescu, B. Jurca, A. Ianculescu, O. Carp, Starch – A suitable fuel in new low-temperature combustion-based synthesis of zinc aluminate oxides, Polyhedron. 30 (2011) 2824–2831. https://doi.org/10.1016/j.poly.2011.08.006.

[30] S. Kurajica, J. Popović, E. Tkalčec, B. Gržeta, V. Mandić, The effect of annealing temperature on the structure and optical properties of sol–gel derived nanocrystalline cobalt aluminate spinel, Mater. Chem. Phys. 135 (2012) 587–593. https://doi.org/10.1016/j.matchemphys.2012.05.030.

[31] N.D. Johari, Z.M. Rosli, J.M. Juoi, S.A. Yazid, Comparison on the TiO_2 crystalline phases deposited via dip and spin coating using green sol–gel route, J. Mater. Res. Technol. 8 (2019) 2350–2358. https://doi.org/10.1016/j.jmrt.2019.04.018.

[32] Y. El Jabbar, H. Lakhlifi, R. El Ouatib, L. Er-Rakho, S. Guillemet-Fritsch, B. Durand, Structure, microstructure, optical and magnetic properties of cobalt aluminate

nanopowders obtained by sol-gel process, J. Non-Cryst. Solids. 542 (2020) 120115. https://doi.org/10.1016/j.jnoncrysol.2020.120115.

[33] S. Zhao, J. Guo, W. Li, H. Guo, B. You, Fabrication of cobalt aluminate nanopigments by coprecipitation method in threonine waterborne solution, Dyes Pigments. 151 (2018) 130–139. https://doi.org/10.1016/j.dyepig.2017.12.062.

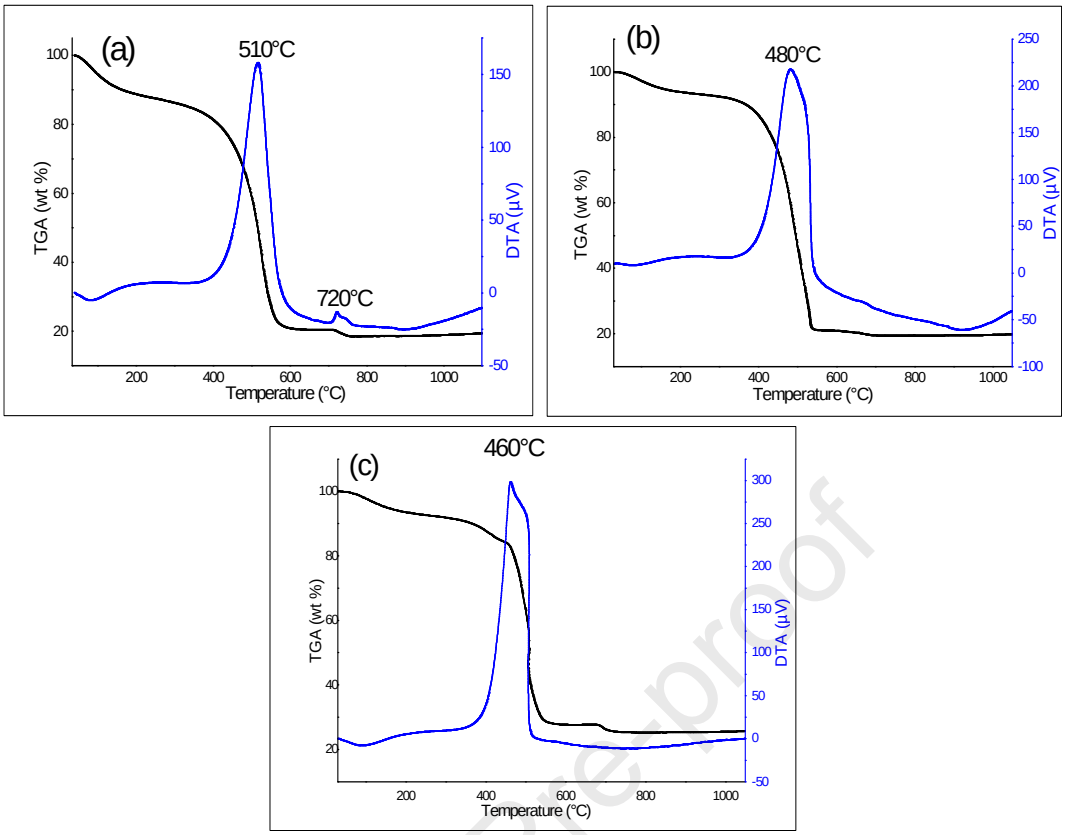

Fig.1. Thermal analysis (TGA-DTA) curves of $Zn_{1-x}Co_xAl_2O_4$ precursors precalcined at 300°C for 12h, (a) x=0, (b) x=0.5 and (c) x=1.

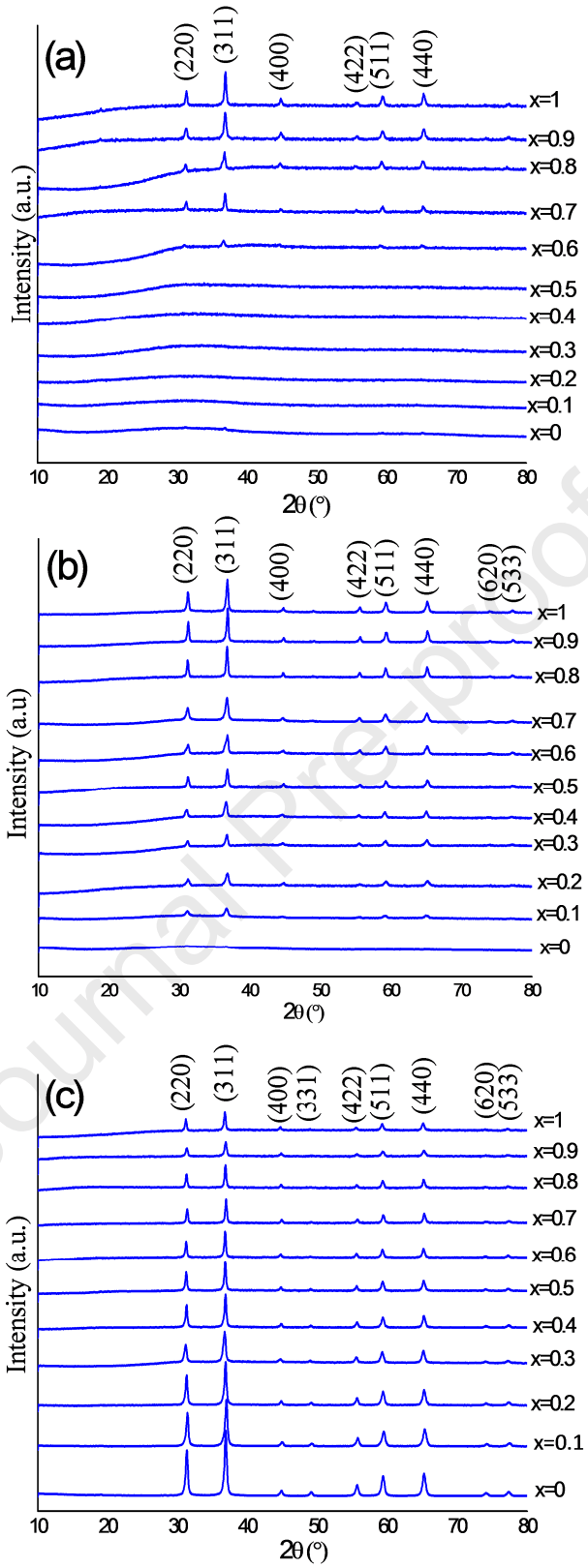

Fig. 2. X-ray powder diffraction patterns of the samples obtained at 500°C (a), 600°C (b) and 700°C (c).

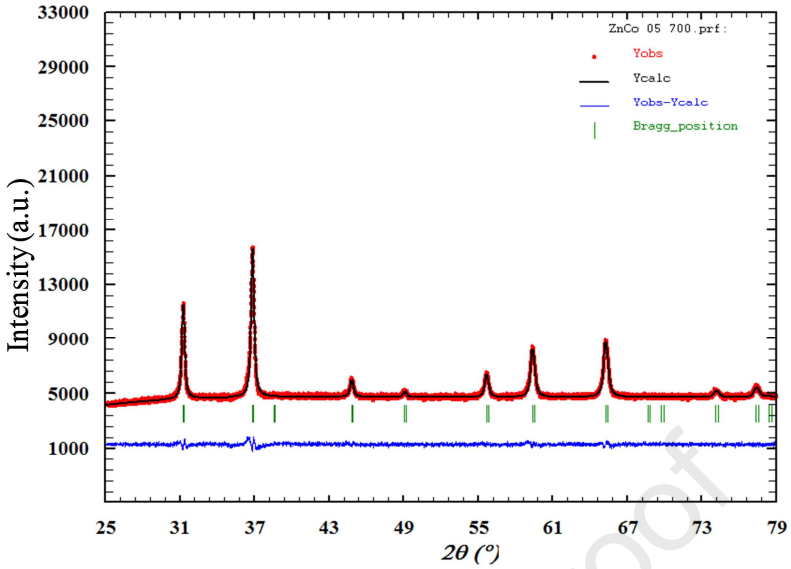

Fig.3. Experimental, calculated and difference signals for $Zn_{0.5}Co_{0.5}Al_2O_4$ sample prepared at 700°C.

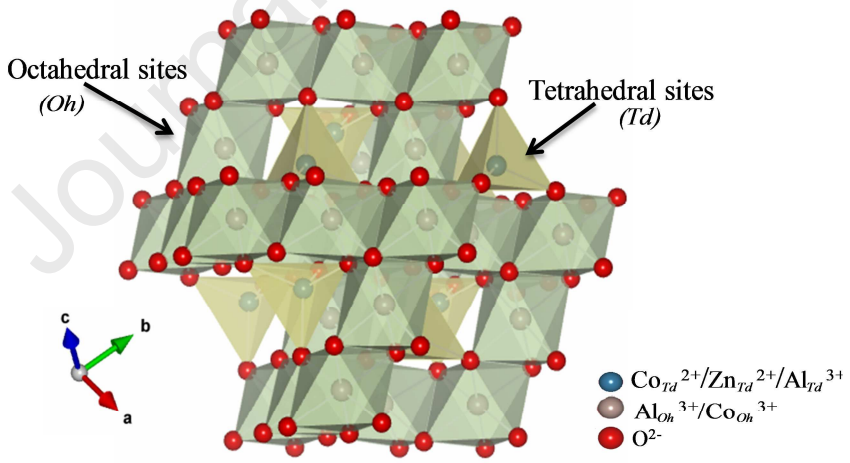

Fig.4. Spinel structure from Riteveld refinement data for $Zn_{0.5}Co_{0.5}Al_2O_4$ composition.

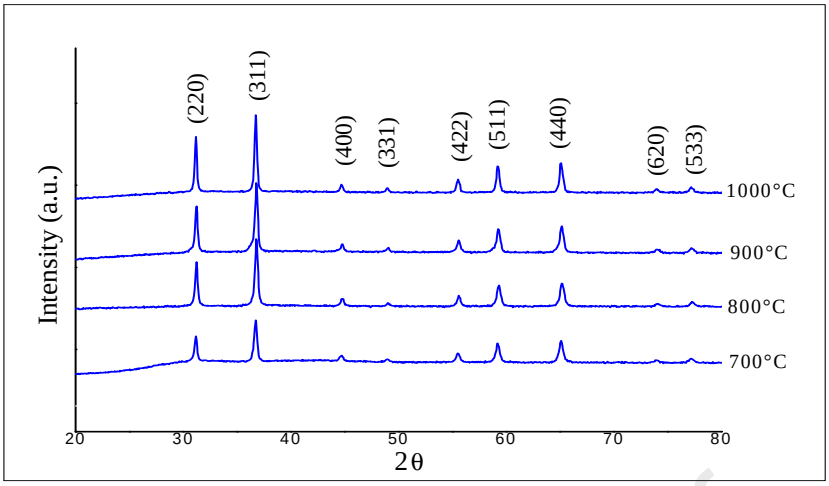

Fig.5. XRD patterns of $Zn_{0.5}Co_{0.5}Al_2O_4$ compound as a function of the calcination temperature.

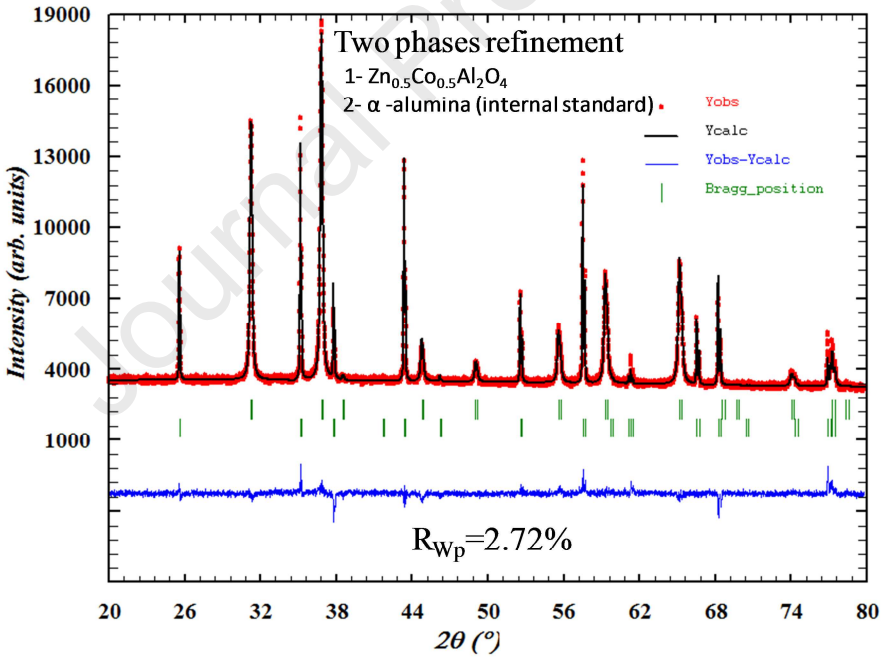

Fig.6. Rietveld refined XRD pattern of $Zn_{0.5}Co_{0.5}Al_2O_4$ sample prepared at 700°C and mixed with α-alumina as internal standard.

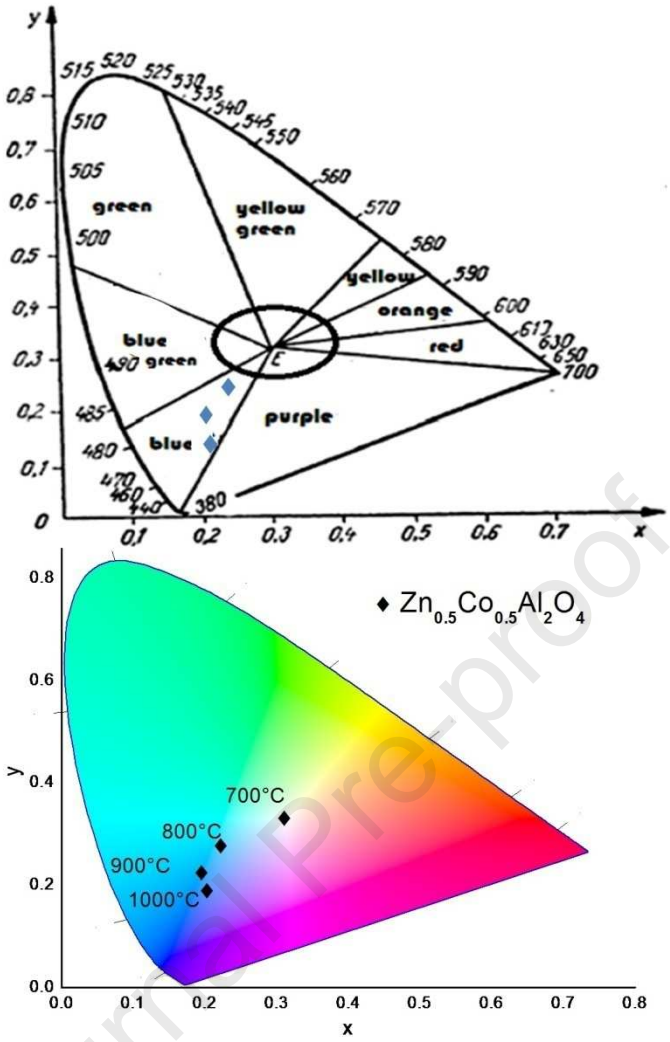

Fig.7. CIE Chromaticity diagram of the $Zn_{0.5}Co_{0.5}Al_2O_4$ powders obtained at different temperature.

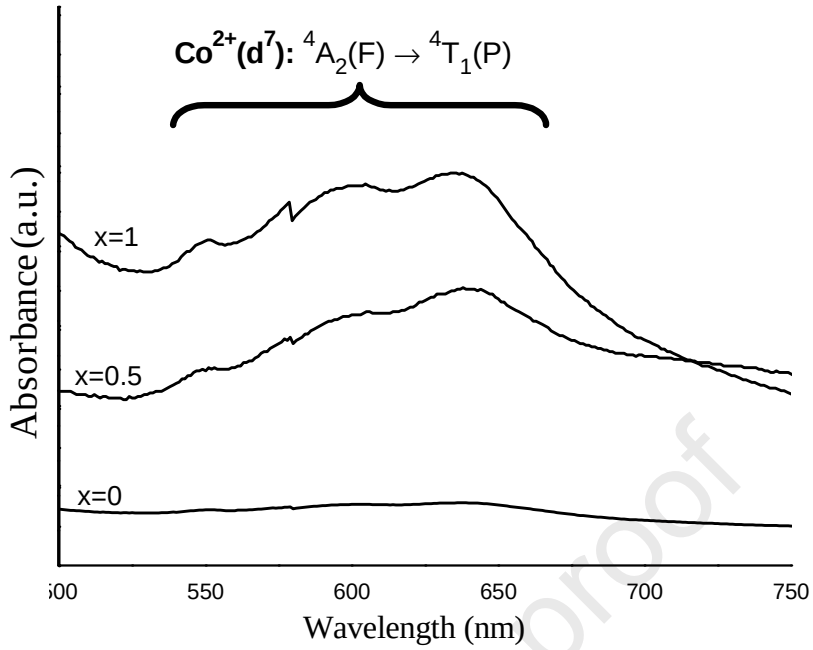

Fig.8. UV-vis spectra of $Zn_{1-x}Co_xAl_2O_4$ (x=0, 0.5, 1) powdered samples obtained at 800°C.

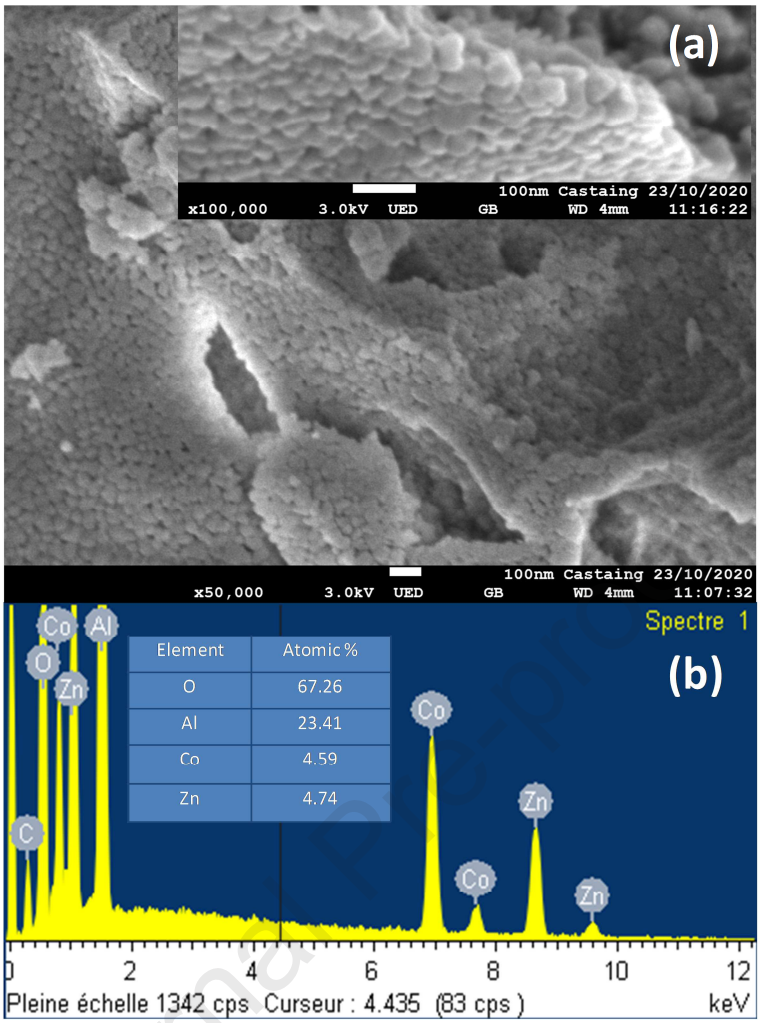

Fig.9. (a) FESEM micrographs (a) and EDS pattern (b) of $Zn_{0.5}Co_{0.5}Al_2O_4$ powder obtained at 800°C

Table 1
Rietveld refinement for $Zn_{1-x}Co_xAl_2O_4$ (x=0; 0.5 and 1) obtained at 700°C

Sample	Atom	Wyckoff Positions x=y=z	Occupancy	Biso	Refinement quality parameters
x=0	Zn	0.125	1.00	0,435 (5)	8.0856 (3) Rp=0.87% Rwp=1.09% χ^2=1.03
	Al	0.500	1.00	0,536 (2)	
	O	0.262(4)	1.00	0,712 (4)	
x=0.5	Co	0.125	0.43	0.899 (3)	8.0833 (3) Rp=1.39% Rwp=1.17% χ^2=1.62%
	Zn	0.125	0.49	0.899 (3)	
	Al	0.125	0.04	0.899 (3)	
	Co	0.500	0.06	0.642 (7)	
	Al	0.500	0.90	0.642 (7)	
	O	0.263(3)	1.00	0.744 (5)	
x=1	Co	0.125	0.85	0.468 (4)	8.0881 (4) Rp=0.93% Rwp=1.16% χ^2=1.07%
	Al	0.125	0.07	0.468 (4)	
	Co	0.500	0.14	0.314 (3)	
	Al	0.500	0.80	0.314 (3)	
	O	0.263(6)	1.00	0.268 (5)	

Table 2
Crystallite sizes (D) and percentage of crystalline phases in $Zn_{0.5}Co_{0.5}Al_2O_4$ sample obtained at different annealing temperatures

T°C	Peaks position 2θ (deg.)			FWHM (deg.)			D (nm)	Crystalline phases (%)
	(311)	(511)	(440)	(311)	(511)	(440)		
700	36.74	59.24	65.13	0.35	0.45	0.51	20	87.92
800	36.74	59.24	65.13	0.33	0.39	0.49	23	91.73
900	36.75	59.25	65.14	0.29	0.36	0.44	25	94.83
1000	36.76	59.26	65.14	0.26	0.34	0.36	26	96.75

Table 3
Evolution of chromatic coordinates (L* a* and b*) of $Zn_{1-x}Co_xAl_2O_4$ (x=0; 0.5 and 1) powders as a function of the calcination temperature.

T (°C)	L*			a*			b*		
	x=0	x=0.5	x=1	x=0	x=0.5	x=1	x=0	x=0.5	x=1
700°C	89.67	30.70	30.20	-2.70	-2.25	-2	12.97	0.61	-0.5
800°C	91.9	31.83	33.78	-1.78	-2.2	-1.23	2.75	-20.63	-15.76
900°C	93.25	35.31	34.11	-1.77	-4.7	-1.21	0.67	-30.12	-22.3
1000°C	93.55	36.01	34.75	-1.55	6.52	2.62	0.27	-38.89	-33.63

Table 4
Specific surface area measurements for $Zn_{1-x}Co_xAl_2O_4$ (x=0.5; 1) at different temperature.

T (°C)	Specific surface area (m^2/g)	
	x=0.5	x=1
800°C	76	45
900°C	35	31
1000°C	23	16

Table 1
Rietveld refinement for $Zn_{1-x}Co_xAl_2O_4$ (x=0; 0.5 and 1) obtained at 700°C

Sample	Atom	Wyckoff Positions x=y=z	Occupancy	Biso	Refinement quality parameters
x=0	Zn	0.125	1.00	0,435 (5)	8.0856 (3) Rp=0.87% Rwp=1.09% χ^2=1.03
	Al	0.500	1.00	0,536 (2)	
	O	0.262(4)	1.00	0,712 (4)	
x=0.5	Co	0.125	0.43	0.899 (3)	8.0833 (3) Rp=1.39% Rwp=1.17% χ^2=1.62%
	Zn	0.125	0.49	0.899 (3)	
	Al	0.125	0.04	0.899 (3)	
	Co	0.500	0.06	0.642 (7)	
	Al	0.500	0.90	0.642 (7)	
	O	0.263(3)	1.00	0.744 (5)	
x=1	Co	0.125	0.85	0.468 (4)	8.0881 (4) Rp=0.93% Rwp=1.16% χ^2=1.07%
	Al	0.125	0.07	0.468 (4)	
	Co	0.500	0.14	0.314 (3)	
	Al	0.500	0.80	0.314 (3)	
	O	0.263(6)	1.00	0.268 (5)	

Table 2
Crystallite sizes (D) and percentage of crystalline phases in $Zn_{0.5}Co_{0.5}Al_2O_4$ sample obtained at different annealing temperatures

T°C	Peaks position 2θ (deg.)			FWHM (deg.)			D (nm)	Crystalline phases (%)
	(311)	(511)	(440)	(311)	(511)	(440)		
700	36.74	59.24	65.13	0.35	0.45	0.51	20	87.92
800	36.74	59.24	65.13	0.33	0.39	0.49	23	91.73
900	36.75	59.25	65.14	0.29	0.36	0.44	25	94.83
1000	36.76	59.26	65.14	0.26	0.34	0.36	26	96.75

Table 3
Evolution of chromatic coordinates (L* a* and b*) of $Zn_{1-x}Co_xAl_2O_4$ (x=0; 0.5 and 1) powders as a function of the calcination temperature.

T (°C)	L*			a*			b*		
	x=0	x=0.5	x=1	x=0	x=0.5	x=1	x=0	x=0.5	x=1
700°C	89.67	30.70	30.20	-2.70	-2.25	-2	12.97	0.61	-0.5
800°C	91.9	31.83	33.78	-1.78	-2.2	-1.23	2.75	-20.63	-15.76
900°C	93.25	35.31	34.11	-1.77	-4.7	-1.21	0.67	-30.12	-22.3
1000°C	93.55	36.01	34.75	-1.55	6.52	2.62	0.27	-38.89	-33.63

Table 4
Specific surface area measurements for $Zn_{1-x}Co_xAl_2O_4$ (x=0.5; 1) at different temperature.

T (°C)	Specific surface area (m^2/g)	
	x=0.5	x=1
800°C	76	45
900°C	35	31
1000°C	23	16

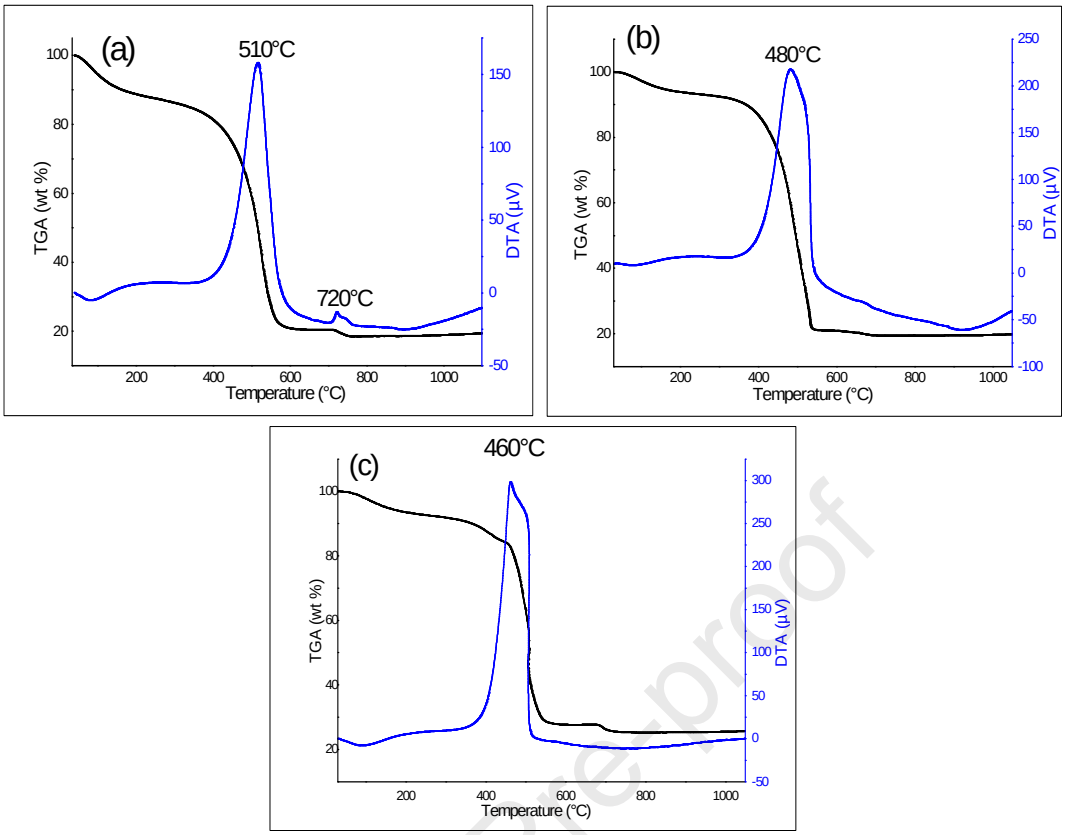

Fig.1. Thermal analysis (TGA-DTA) curves of $Zn_{1-x}Co_xAl_2O_4$ precursors precalcined at 300°C for 12h, (a) x=0, (b) x=0.5 and (c) x=1.

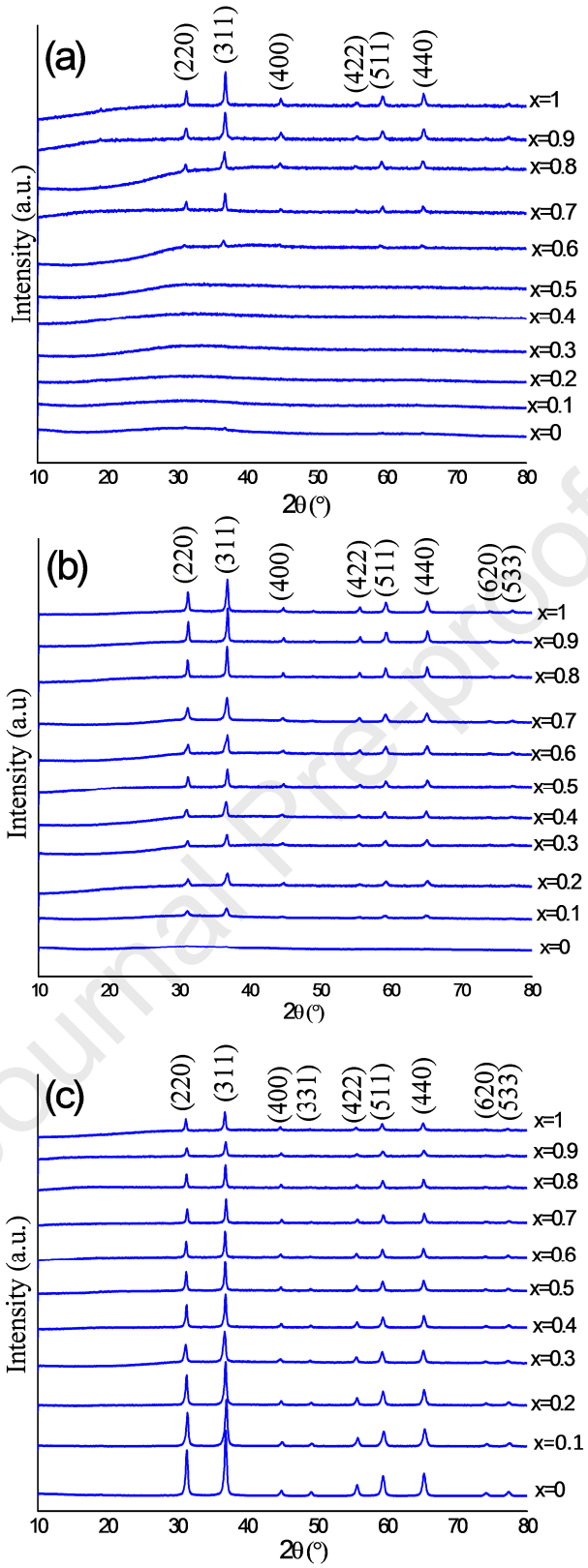

Fig. 2. X-ray powder diffraction patterns of the samples obtained at 500°C (a), 600°C (b) and 700°C (c).

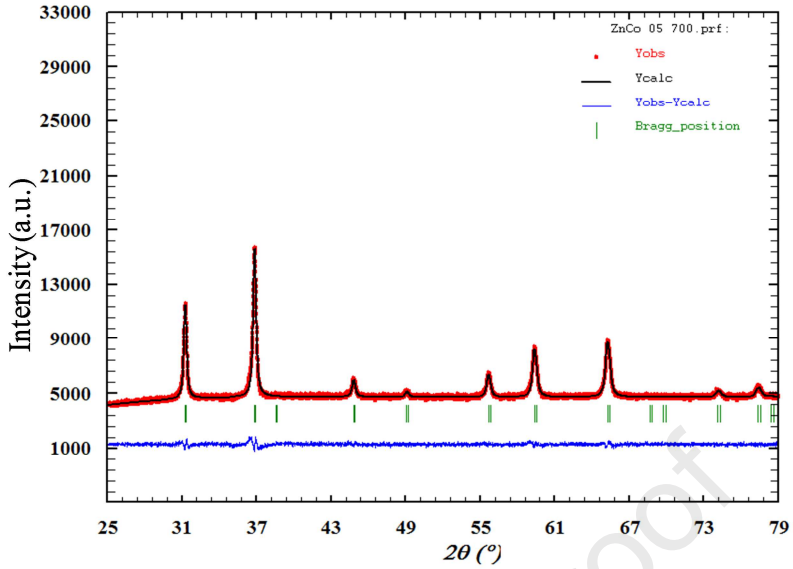

Fig.3. Experimental, calculated and difference signals for $Zn_{0.5}Co_{0.5}Al_2O_4$ sample prepared at 700°C.

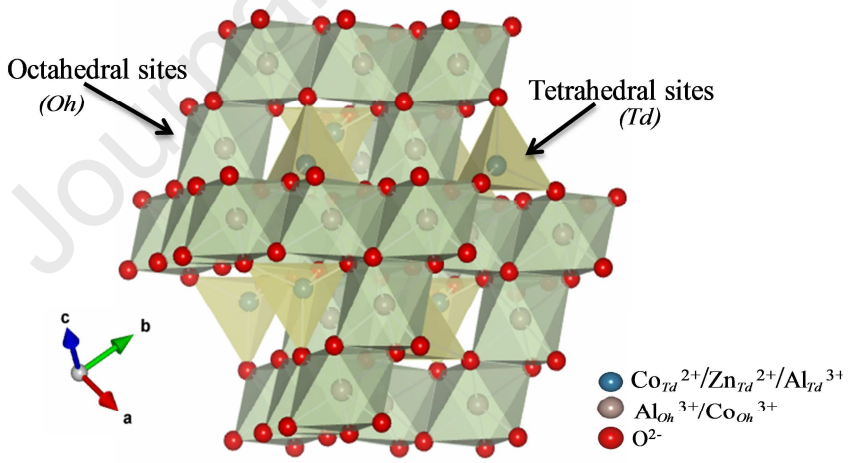

Fig.4. Spinel structure from Riteveld refinement data for $Zn_{0.5}Co_{0.5}Al_2O_4$ composition.

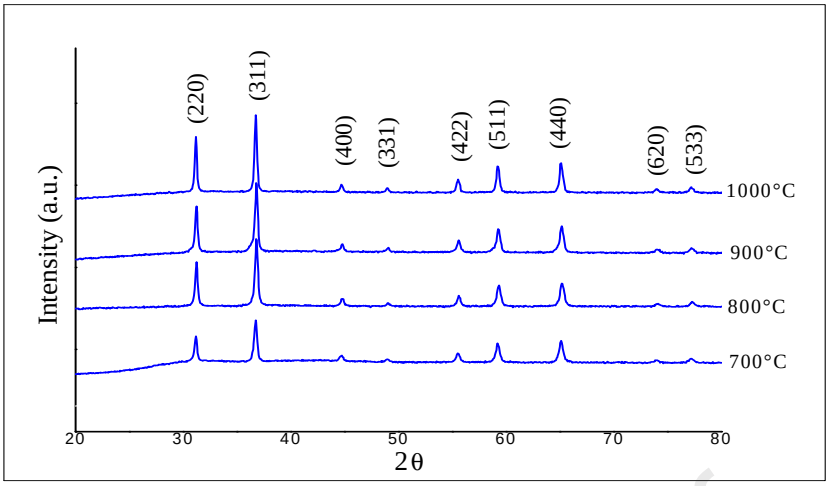

Fig.5. XRD patterns of $Zn_{0.5}Co_{0.5}Al_2O_4$ compound as a function of the calcination temperature.

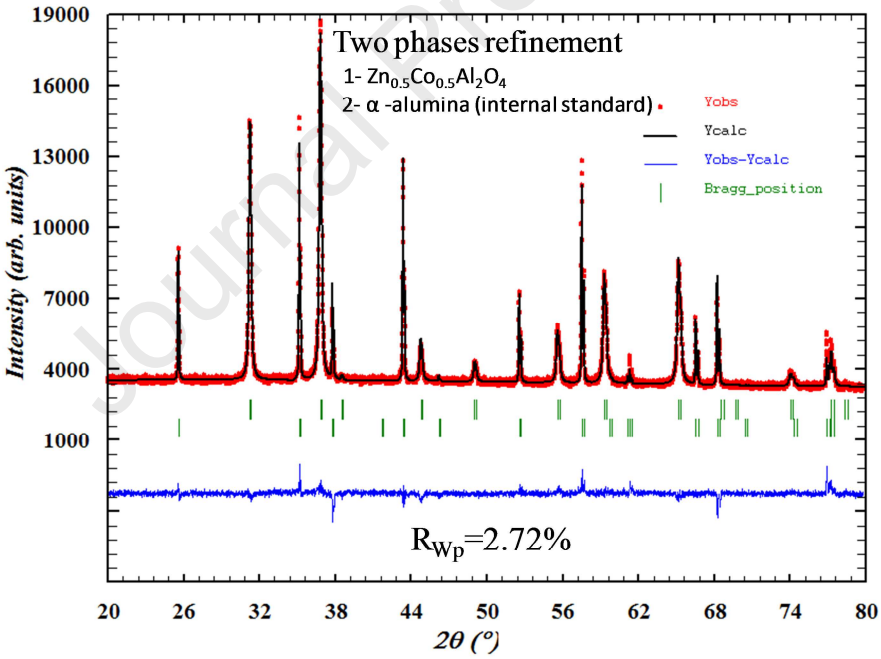

Fig.6. Rietveld refined XRD pattern of $Zn_{0.5}Co_{0.5}Al_2O_4$ sample prepared at 700°C and mixed with α-alumina as internal standard.

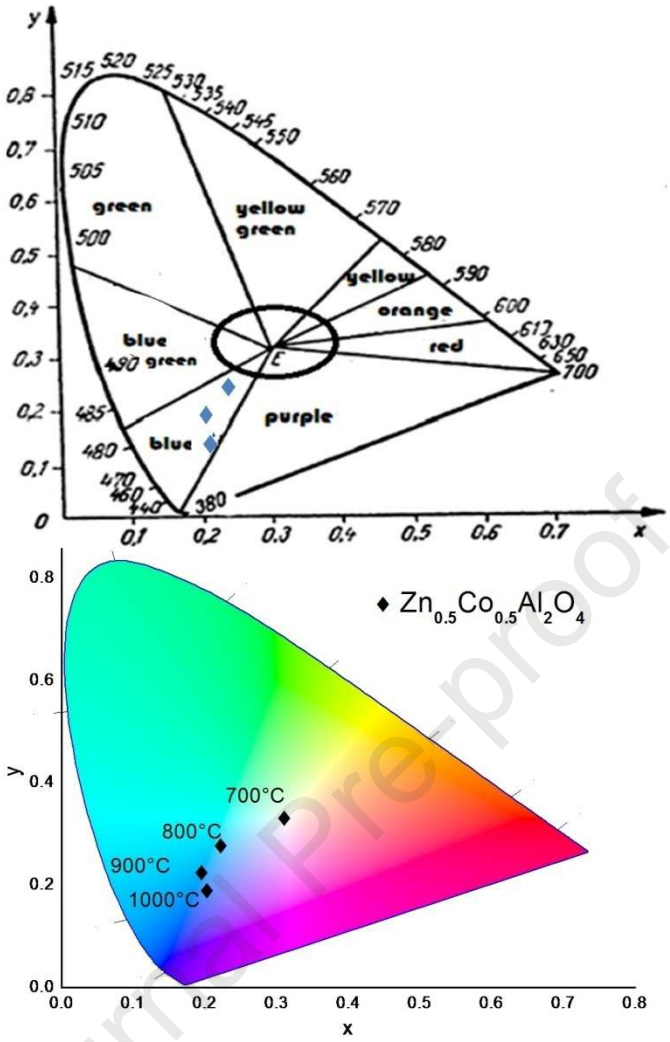

Fig.7. CIE Chromaticity diagram of the $Zn_{0.5}Co_{0.5}Al_2O_4$ powders obtained at different temperature.

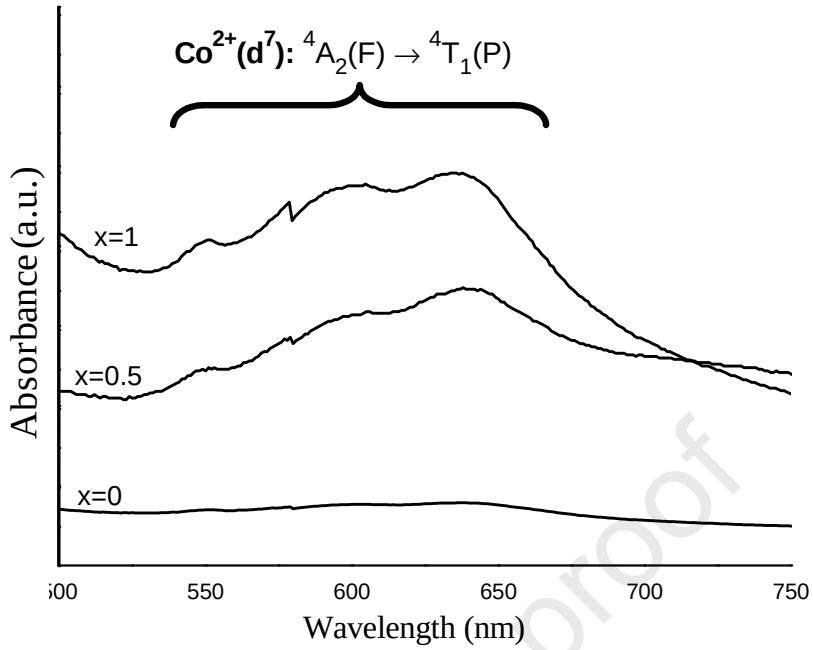

Fig.8. UV-vis spectra of $Zn_{1-x}Co_xAl_2O_4$ (x=0, 0.5, 1) powdered samples obtained at 800°C.

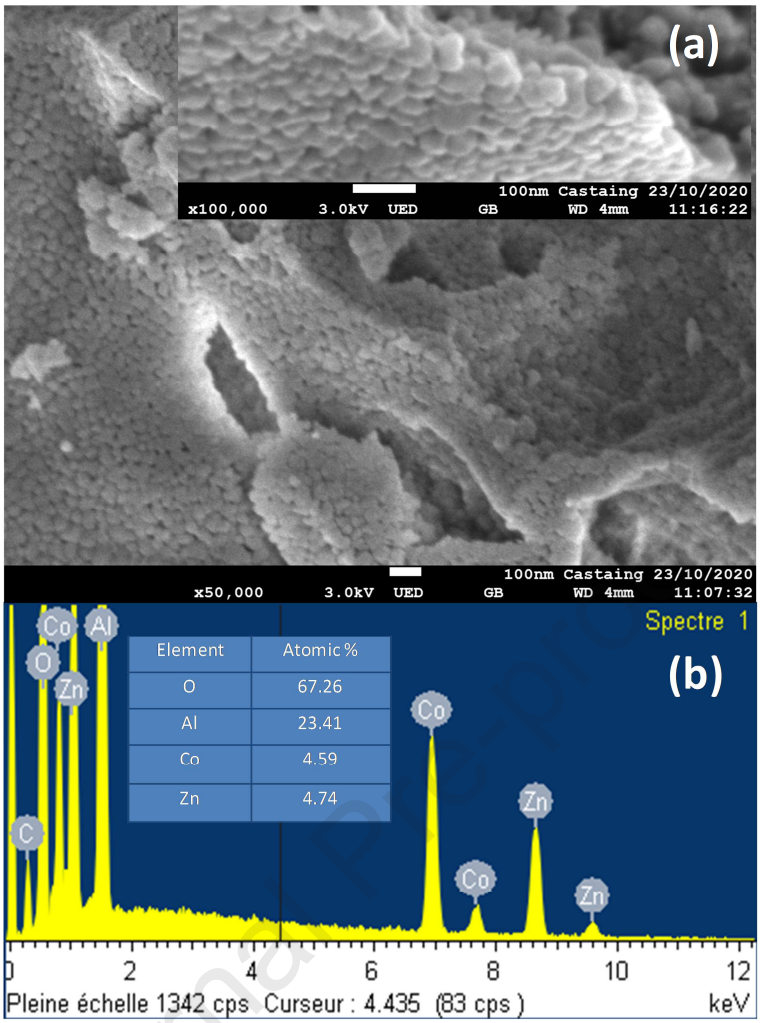

Fig.9. (a) FESEM micrographs (a) and EDS pattern (b) of $Zn_{0.5}Co_{0.5}Al_2O_4$ powder obtained at 800°C